Available online at www.elixirpublishers.com (Elixir International Journal)

Mechanical Engineering

Elixir Mech. Engg. 102 (2017) 44428-44433

ISSN: 2229-712X

CFD Analysis of Centrifugal Air Compressor for Turbocharged IC Engine

Vivek V. Kulkarni[1], Dr. Anil T.R.[1] and Dr. Rajan N.K.S.[2]

[1]Department of Mechanical Engineering, KLS Gogte Institute of Technology, Belgaum, Karnataka State, India.

[2]Department of Aerospace Engineering, CGPL, Indian Institute of Science (IISc), Bangalore, Karnataka State, India.

ARTICLE INFO

Article history:

Received: 21 December 2016;

Received in revised form: 18 January 2017;

Accepted: 25 January 2017;

Keywords

Producer gas,
Centrifugal compressor,
Pressure ratio,
Mass flow rate,
Computational Fluid Dynamics (CFD).

ABSTRACT

Compressor characteristics, being representations of the compressor pressure ratio as a function of gas flow through the compressor have been studied. Compressors are used in turbochargers to increase the pressure of air and also its density greater than ambient. Choosing the right compressor is very important in obtaining best power output of engine by turbocharging, so it is important to have compressor map for matching turbocharger with a particular engine. Compressor map is drawn by running compressor at varying speeds and mass flows. In this paper compressor characteristics were investigated through CFD analysis.

Introduction

Besides the pressurization and transportation of fluids in the process and chemical industries, other applications of centrifugal compressors involve fluid compression for use in aircraft engines, in industrial gas turbines and in turbocharged combustion engines [1]. Centrifugal compressors have an instable working region. In this region, a decrease of flow results in a decrease of outlet pressure. When the plenum pressure behind the compressor is higher than the compressor outlet pressure, the fluid tends to reverse or even flow back in the compressor.

As a consequence, the plenum pressure will decrease, inlet pressure will increase and the flow reverses again. This phenomenon, called surge, repeats and occurs in cycles with frequencies varying from 1 to 2 Hz [2]. Another aerodynamic instability that can occur in centrifugal compressors is stall. Both instabilities dramatically decrease the efficiency and severe surge can even cause mechanical damage to the compressor.

The working principle of a centrifugal compressor is to increase the kinetic energy of the fluid with a rotating impeller. The fluid is then slowed down in a volume called the plenum, where the kinetic energy is converted into potential energy in the form of a pressure rise. Hence compression is achieved by transferring momentum to the fluid and the subsequent diffusion to convert the kinetic energy into pressure. The momentum transfer takes place at the curved blades of the impeller that is mounted on a rotating shaft. Diffusion takes place in the annular channel of increasing radius around the impeller, usually referred to as diffuser [3]. Figure 1 shows the sketch of a centrifugal compressor, which consists of a stationary casing, containing a rotating *impeller* that imparts a high velocity to the fluid, and a number of fixed diverging passages in which the fluid is decelerated with a consequent rise in static pressure in the plenum.

The latter process is one of diffusion, and thus the part of the compressor containing the diverging passages is known as the *diffuser*. Fluid enters the impeller eye and is whirled around at high rotational speed (by the vanes or without the vanes) on the impeller disc.

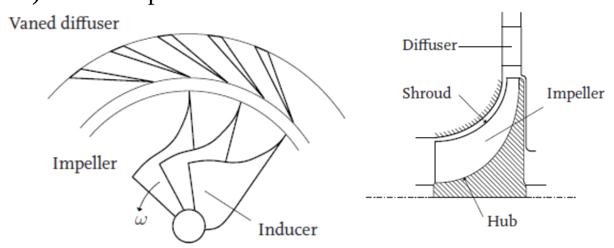

Figure 1. Sketch of Centrifugal Compressor [3].

The static pressure rise is obtained in the diffuser, where very high velocity of the fluid, leaving the impeller tip, is reduced to a velocity similar to the velocity of the fluid entering the impeller eye [2]. In general, the mechanical and thermodynamic processes in a turbo-compressor are described by the continuity equation, the momentum equation, and the first and second law of thermodynamics. However, applying these general principles to the real flow in centrifugal compressors, being three-dimensional, unsteady and viscous, is extremely difficult [3].

The function of a compressor is to pressurize a fluid. The compressor characteristics are visualized in a compressor map. The *surge line* connects points from whereon surge can occur. Surge is associated with a drop in delivery pressure, and with violent aerodynamic pulsations that are transmitted throughout the whole machine. As visualized in Fig. 2, the part left of the surge line has positive slope and this is the region where surge can occur. A safety margin is taken into account, resulting in a new line called the *surge avoidance line.* The task of the surge avoidance controller is to prevent the compressor from operating in a point in the compressor map that is located to

Tele: +91-09448014163
E-mail address: vvkulkarni@git.edu

the left of the surge avoidance line [2]. The individual characteristic curves or speed lines are formed by steady-state operating points with the same rotational speed. The achievable flow rates are limited by the occurrence of surge at low flows and the phenomenon known as choking at high flows.

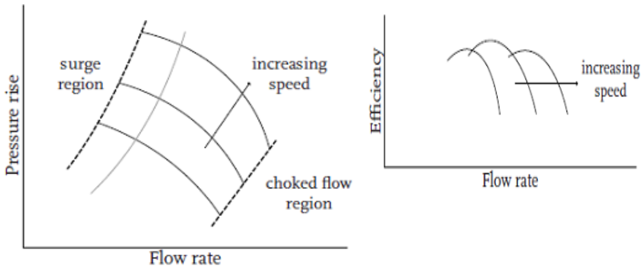

Figure 2. Schematic representation of a compressor map [2]

Choking occurs when the local velocity, usually in the impeller exit or diffuser, reaches the speed of sound.

Modeling and Grid Generation

The impeller considered in the present study consists of 8 main blades and 8 splitter blades. The tip clearance between the blade tip and shroud surface is 0.1mm. The impeller geometry was designed using BladeGen workbench in ANSYS 13V.

Table 1. Details of impeller geometry

Blade information	Backward swept
No. of blades (main+splitter)	8+8
Eye radius, r_e	8.8 mm
Eye tip radius, r_t	24.42 mm
Impeller exit radius, r_i	36.4 mm
Blade height at impeller exit, h_e	4.67 mm
Hub beta at LE, β_{h1}	14.7^0
Tip beta at LE, β_{t1}	50.5^0
Hub beta at TE, β_{h2}	19.1^0
Tip beta at TE, β_{t2}	17.1^0

The details of impeller geometry are shown in Table 1. Fig. 3 shows the 3D view of impeller obtained by dimensions mentioned in Table1 and the larger blade is the main blade and the smaller blade is splitter blade. To reduce the computation time, one passage of the blade consisting of one main blade and one splitter blade is meshed and solved by applying periodic boundary conditions at each side of blade passage.

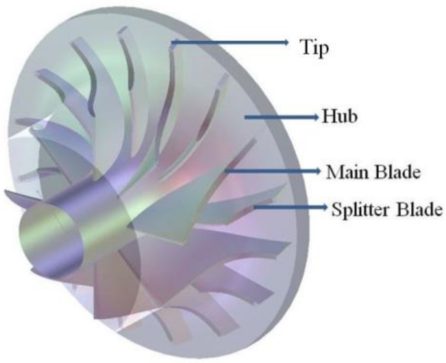

Figure 3. Modeled view of an impeller in isometric view.

The grid is generated using TurboGrid workbench approach in ANSYS 13. It consists of hexahedral cells of HJCL-type of grid with O-grid around the blades. There are 493521 nodes in a passage which includes one main blade and one splitter blade with periodic boundary conditions. Fig. 4 shows grid generated to one passage of impeller.

The boundary conditions applied are total pressure and total temperature at inlet and mass flow at outlet and the impeller rotation speeds were also specified.

The CFD solver used is CFX which is commercially available CFD software and the boundary conditions used are P-total and T-Total at inlet and mass flow rate at outlet. The standard Shear Stress Transport (SST) k-ω turbulence model is used for. The residual target set for the simulation is $1e^{-6}$ and at lower mass flow rates the convergence achieved was between $1e^{-3}$ and $1e^{-6}$.

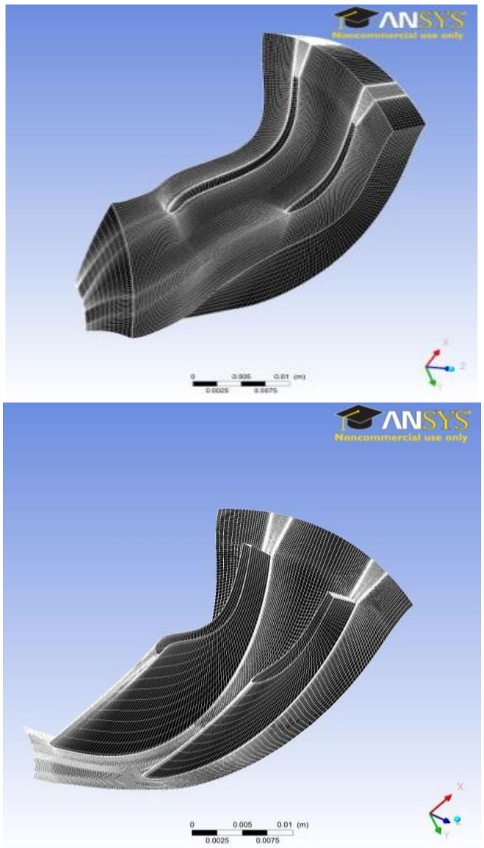

Figure 4. Mesh generated on impeller passage (top) and over blades (bottom)

The simulations with these boundary conditions are obtained for varying speeds and different parameters like impeller isentropic efficiency, total pressure ratio (P_r) are plotted at different mass flow rates. CFD contour plots and vector plots are also used to understand flow through the impeller and identify the regions of losses.

Volute Design

The depth of volute (scroll) varies along its circumference from first point to the last point, hence the depth is measured at different angular intervals as shown in Table 2 and then the model is generated. The volute was modeled in CATIA-V5 and the details of its geometry are shown in Fig. 5 (top).

Table 2. Details of volute geometry

Angle	Depth in mm
First point	7.5
41.31	8.5
30.17	13.5
27.97	17.5
23.86	18.5
26.57	19.5
30.17	21.5
26.35	23.5
40.48	27.5
42.88	32.5
32.26	36.5

The volute was meshed with unstructured tetrahedral mesh in ICEM CFD. Fig. 5(bottom) shows the unstructured tetrahedral mesh generated on volute. There are 493521 nodes with 459360 hexahedral elements in impeller and 1367117 tetrahedral elements in volute.

Boundary Condition

There are two separate set of simulations carried out in the present study. As first case flow through only impeller is studied and then the volute is attached by creating interface between impeller and volute and the flow parameters are studied. CFX provides the option to create domain interface between rotor and stator components in CFX pre.

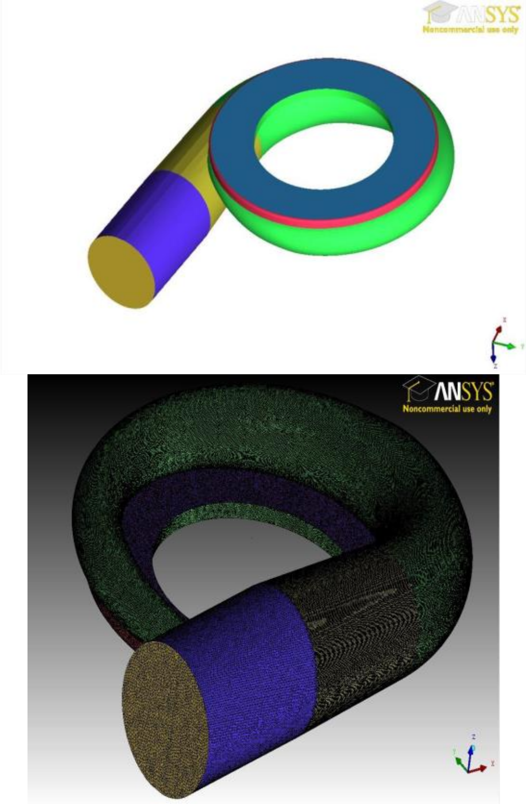

Figure 5. Modeled view of volute (top) and unstructured mesh on volute (bottom).

In the second case i.e. for the interface case, P-total at inlet and opening type of boundary was applied at outlet of volute. Fluid to fluid interface was created between impeller and volute. As described earlier it is multiple domain flow problem. The convergence criteria set for residuals is $1e^{-6}$. However at off design points where flow separation takes place and flow reversal occurs at the blades and the convergence achieved was between $1e^{-3}$ and $1e^{-6}$. All the walls are set as smooth walls with no slip wall condition. Fig. 6 shows the sketches for impeller and volute case, after applying the above conditions.

A set of results were obtained after running the compressor for different speeds. The various plots were plotted in CFX-post to understand the flow and performance characteristics of the compressor. In this paper, the discussion is carried out on the plots obtained for impeller without volute and impeller with volute.

The flow through compressor impeller was solved for different speed starting from 40000 rpm to 50000 rpm with total pressure at inlet and mass flow boundary at outlet. The Fig 7 shows the contours of total pressure and velocity across the impeller blade in blade to blade view for $\dot{m} = 0.11$ kg/s and N = 60000 rpm.

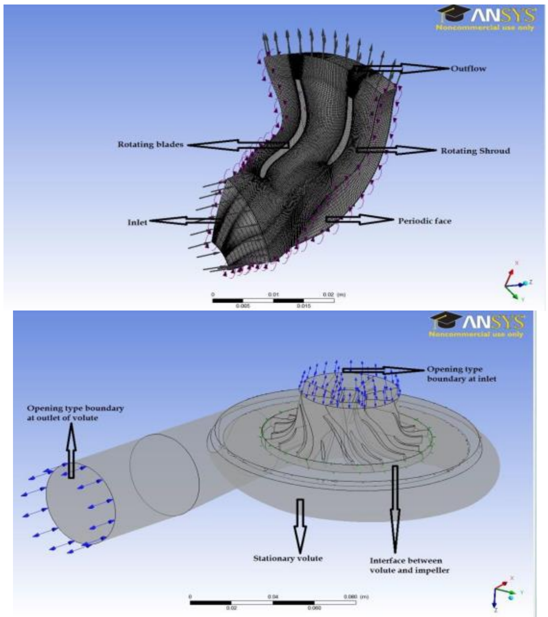

Figure 6. Boundary conditions applied for impeller without volute (top) and impeller with volute (bottom).

Results and Discussions

It can be seen from the plot that the pressure increases from leading edge to trailing edge and a low pressure region exists at just downstream of the of the leading edge which is due to flow separation at lower mass flow rates for given speed which results in stalling.

This signifies the increase in total pressure due to increase in velocity of the air which in turn due to energy transfers from rotating blade to flowing air from leading edge to trailing edge. In diffuser by converting this part of kinetic energy into pressure energy the total pressure can be increased substantially.

When a gas is compressed its density and also the temperature increases as shown in Fig. 8. Normally, in centrifugal compressors, as the mass low rate is reduced below a critical value for any given rotational speed, the flow separation from blade takes place and results in stalling which later leads to surge or compressor instability.

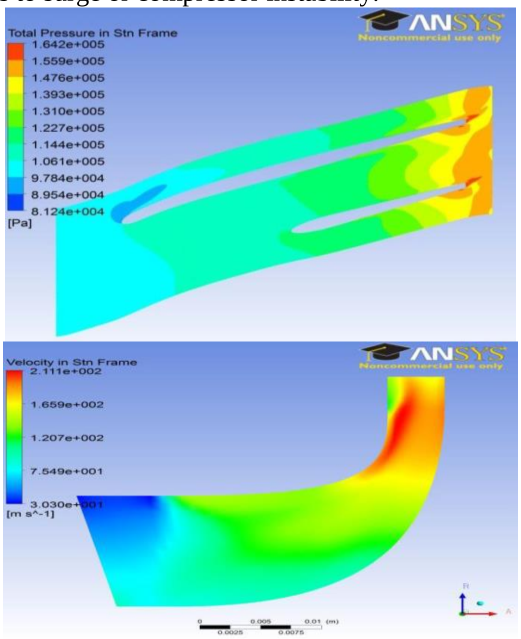

Figure 7. Contours of total pressure (top) and velocity (bottom) for $\dot{m} = 0.11$ kg/s and N = 60000 rpm at span of 0.5.

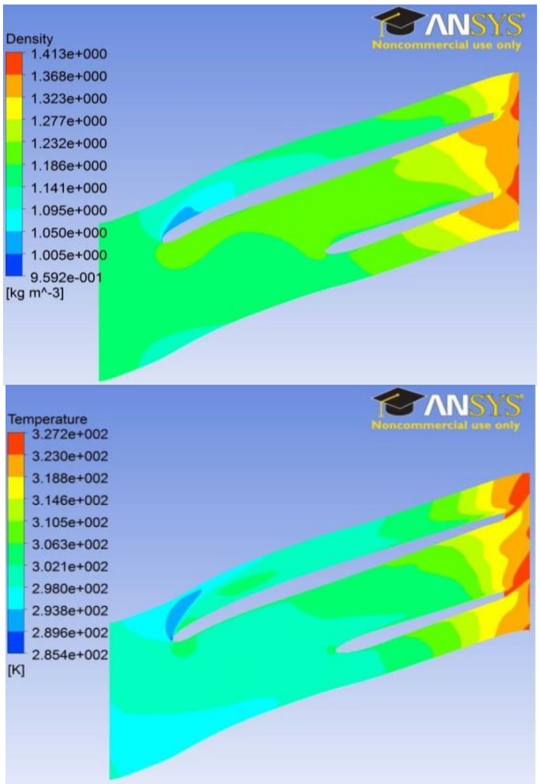

Figure 8. Contours of density (top) and temperature (bottom) for ṁ = 0.11 kg/s and N = 60000 rpm at a span of 0.5.

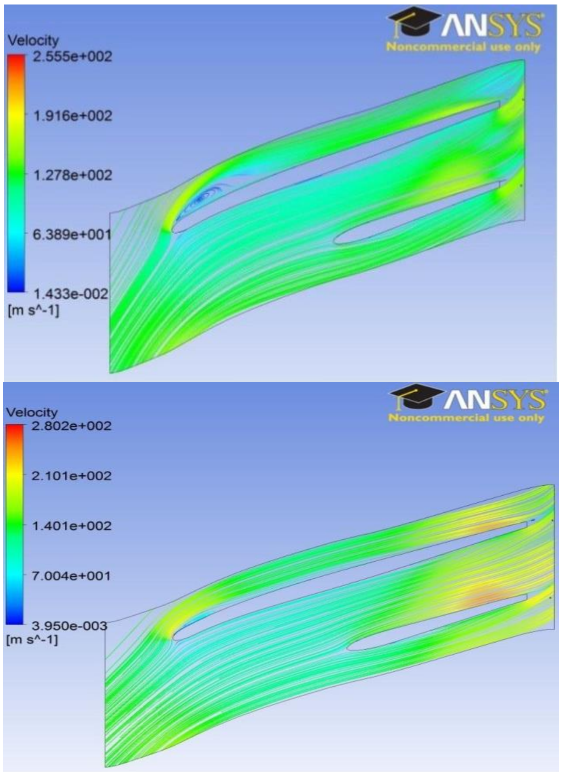

Figure 9. Velocity streamlines for ṁ = 0.11 kg/s (top) and ṁ = 0.16 kg/s (bottom) at N = 60000 rpm at a span of 0.5.

Figure 9 shows the streamlines for ṁ = 0.11 kg/s and ṁ = 0.16 kg/s respectively. It can be observed that for ṁ = 0.11 kg/s, the flow separation occurs after the leading edge and it does not exists for ṁ = 0.16 kg/s. This flow separation is shown in 3D view in Fig. 10 (top).

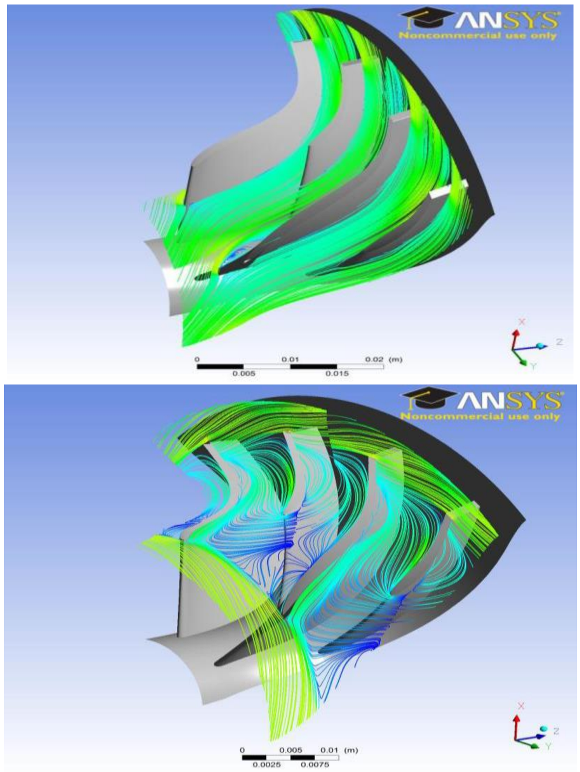

Figure 10. Flow separation near leading edge (top) and tip leakage (bottom) for ṁ = 0.11 kg/s and N = 60000 rpm.

In un-shrouded centrifugal compressors, a tip leakage flow occurs due to pressure difference between forward face (pressure surface) and rear face (suction surface) and is shown in Fig. 10(b). This results in specific work reduction for any compressor and hence the tip clearance must be kept as low as possible and is limited by manufacturing constraints.

Characteristic Maps for Compressor

The graphs were plotted with different mass flow rates vs. pressure ratios and different mass flow rates vs. isentropic efficiencies developed by compressor at different speeds and are shown in Fig. 11. From Fig. 11(top), it can be observed that the mass flow rate that the impeller can handle increases with the increase in its rotational speed i.e. at 40000 rpm the maximum value of mass flow rate that the impeller can handle is around 0.17 kg/s beyond which the sonic condition is reached and flow chokes and as this rotational speed increases to 80000, the maximum mass flow rate is around 0.19 to 0.2 kg/s and flow chokes beyond this point.

Figure 11(bottom) shows the graph of mass flow rate vs. isentropic efficiency for impeller. It can be observed that at all speeds, there is one maximum efficiency point and the efficiency increases with the increase in mass flow initially and at one point it reaches maximum value and start decreasing with further increase in mass flow. This is because, at peak efficiency point, the gas incidence angle matches with blade angles and with the decrease in mass flow rate gas incidence angles changes and results in flow separation from blade.

While, increase in mass flow rate after the peak efficiency point results in increase in absolute velocity of gas and when it reaches sonic speed, the flow chokes.

Result Plot of Flow through Compressor

When problem is solved by creating interface between rotating impeller and stationary volute, it becomes a multiple domain problem and the presence of volute will cause substantial changes in the performance of compressor.

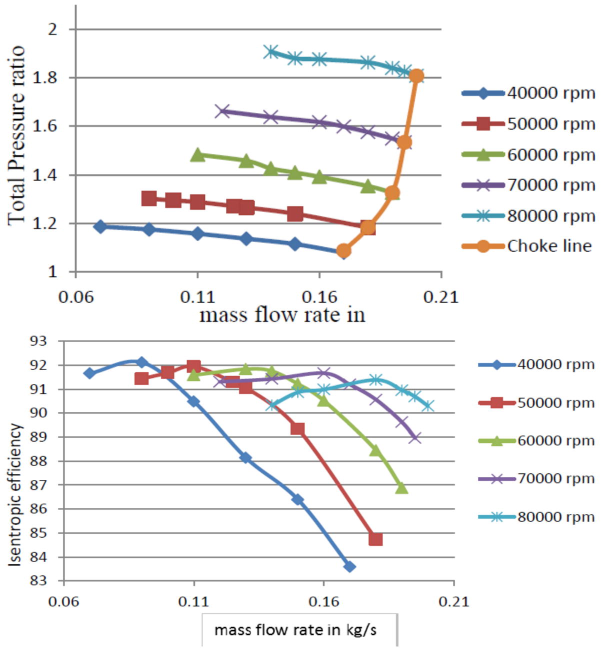

Figure 11. Mass flow rate vs. Total pressure ratio (top) and mass flow rate vs. isentropic efficiency (bottom).

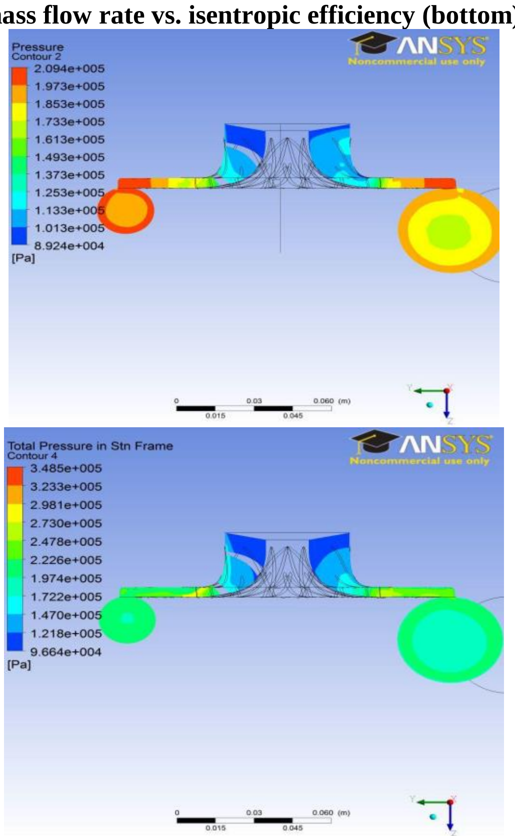

Figure 12. Contours of static pressure (top) and total pressure (bottom), for ṁ = 0.16 kg/s and N=70000 rpm.

Figure 12 shows the contours of static pressure and total pressure in a plane along the axis of the impeller. It can be observed from the plot that as air flows through the impeller its total pressure increases due to increase in kinetic energy of air in the impeller and as air enters the vane-less diffuser, the total pressure decreases. It can be observed from the graphs that the pressure suddenly decreases at some portion in the volute and this is because of air accelerating from smaller area to larger area. As air flows through the diffuser part of volute, the kinetic energy is converted into pressure energy which results in increase of static pressure and decrease in total pressure.

When the flow through only impeller was studied, between 70000 to 80000 rpm, the maximum mass flow rate handled was around 0.195 kg/s. But in this case, the compressor was able to handle mass flow rates up to 0.23 kg/s. This is due to effective diffusion that occurs at downstream of the impeller which could bring down the Mach number and the flow choking was avoided. Fig. 13 shows the contours of Mach number in a plane along the axis (top) and perpendicular to the axis of impeller (bottom). It can be observed that the Mach number decreases at downstream of impeller which is an indication of the effective diffusion taking place in the diffuser there by allowing the compressor to handle higher mass flow rates.

Figure 14 shows the mass flow rate vs. total pressure ratio and mass flow rate vs. isentropic efficiency, at different speeds to predict the operating range of compressor. It can be seen that the same trend follows and after the peak efficiency point the efficiency decreases with the increase or decrease in mass flow rates.

Whereas Figure 15 shows a graph comparing the mass flow rates and static pressures developed at 60000 rpm for impeller without volute and impeller with volute.

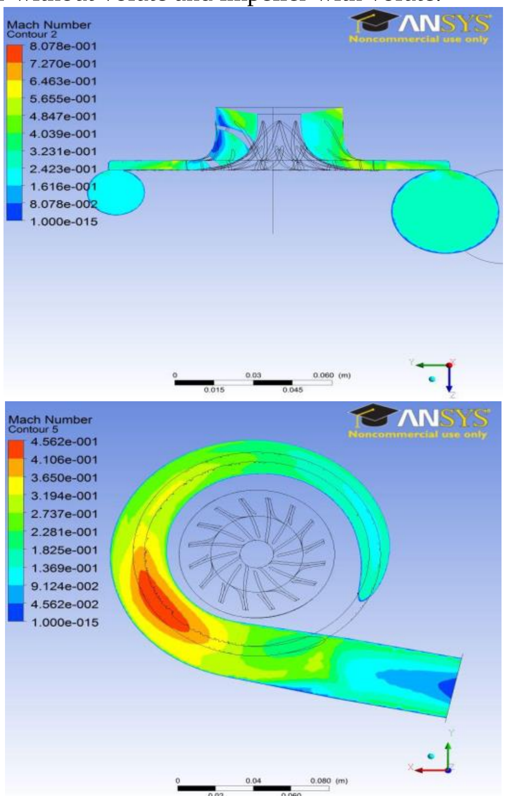

Figure 13. Contours of Mach number in a plane, along the axis (top) and perpendicular to the axis of impeller (bottom), for ṁ = 0.16 kg/s, N=70000 rpm.

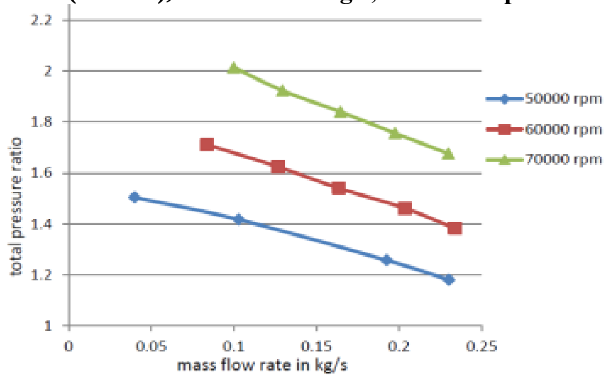

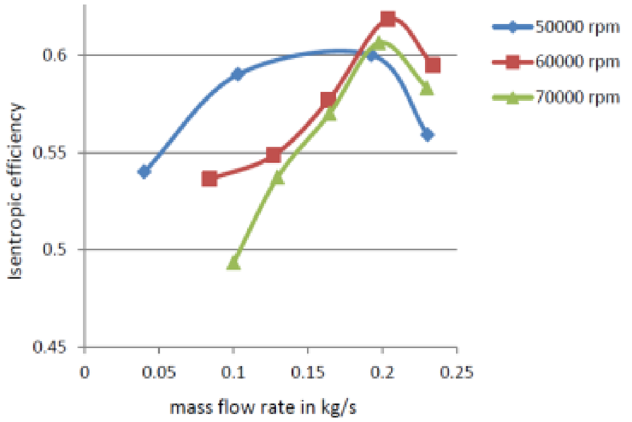

Figure 14. Mass flow rate vs. total pressure ratio (top) and isentropic efficiency (bottom).

As explained earlier we can observe considerable increase in pressure ratio developed and the mass flow handled for impeller with volute when compared to impeller without volute.

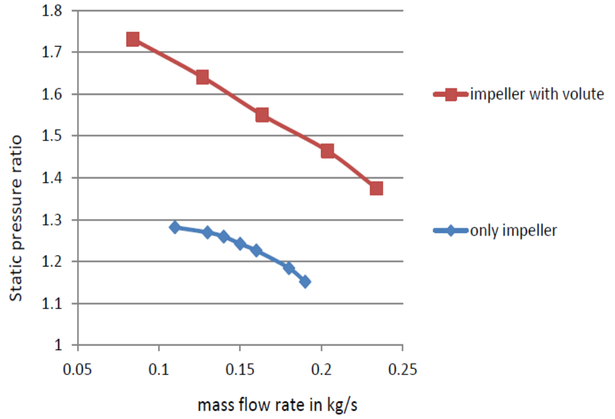

Figure 15. Mass flow rate vs. static pressure ratio comparison.

Conclusions

The CFD simulations were carried out in two different stages, one with only impeller (without volute) and the other by creating interface between impeller and volute (with volute). This helps in understanding the flow characteristics through the impeller. Following are the conclusions drawn:

1. It was observed that, during a flow through impeller, maximum mass flow rate that the impeller could handle was found to be around 0.2 kg/s and beyond this, sonic condition was reached as Mach number reached 1.
2. When volute was attached, the compressor could handle relatively higher mass flow rates due to effective diffusion that was taking place at the downstream of the impeller and the sonic conditions were not reached early.
3. Also because of this diffusion, the kinetic energy available in air at the outlet of impeller was converted into pressure energy and it can be observed from graphs that the static pressure ratio is higher for the second case.
4. It can be observed from the streamline plots and contour plots that due to swirling flow in volute there are some pressure losses due to fluid friction.
5. For the case of impeller with volute, it is observed that the efficiency of impeller and overall efficiency of compressor are lower when compared with the efficiency of impeller without volute. This is because; the compressor has to do more work to push the air through the volute.
6. As the compressor characteristics are plotted at different conditions such as different mass flow rates and speeds, the data can be used for turbocharger analysis and engine matching.

Acknowledgment

Vivek Kulkarni thanks Dr. Anil T.R. and Dr. Rajan N.K.S. for guiding and helping in maintaining the flow of work. The authors also thank Visveswaraya Technological University (VTU), Authorities of KLS Gogte Institute of Technology, Belgaum, Karnataka State, INDIA, for encouraging this paper.

References

[1] Saravanamuttoo, H.I.H., Rogers, G.F.C., Cohen, H. 'Gas Turbine Theory.' 2001.

[2] Peter Tijl, Modeling, simulation and evaluation of a centrifugal compressor with surge avoidance control. DCT 2004.039, Traineeship report.

[3] Jan van Helvoir, Centrifugal Compressor Surge, Modeling and Identification for Control, Technical Universities Eindhoven, 2007– ISBN-13: 978-90-386-1095-5.